archives
of thermodynamics
Vol. **40**(2019), No. 4, 21–48
DOI: 10.24425/ather.2019.130006

Exergy based analysis of solar air heater duct with W-shaped rib roughness on the absorber plate

SUMER SINGH PATEL*
ATUL LANJEWAR

Department of Mechanical Engineering, Maulana Azad National Institute of Technology, Bhopal 462051, Madhya Pradesh, India

Abstract Exergy analysis is a powerful thermodynamic tool and it helps in computing the actual output of a system. It helps the researchers to optimize the roughened solar air heater design to compensate the present and also the future needs. In this study, investigation on exergetic performance evaluation of a solar air heater with W-shaped roughened absorber surface analytically by employing mathematical model and the results obtained are compared with smooth plate solar air heater under same operating conditions. The exergetic efficiency curves has been plotted as a function of different values of Reynolds number and temperature rise parameter for different roughness parameters. The maximum augmentation in the exergetic efficiency of the solar air heater with W-shaped roughened surface as compared to solar air heater with smooth surface has been obtained as 51% corresponding to the relative roughness height of 0.03375 and the rib angle of attack about 60°. Based on the exergetic efficiency the suitable design parameters of solar air heater with W-shaped roughened are determined.

Keywords: Solar air heater; W-shape rib; Exergetic efficiency; Reynolds number; Thermal efficiency; Temperature rise parameter

Nomenclature

A_c – surface area of absorber plate, m^2
C_p – specific heat of air, J/kgK

*Corresponding Author. Email: patelsumer@gmail.com

D_h – hydraulic diameter of duct, m
e – rib height, m
E_{LA} – exergy losses due to absorption of irradiation by absorber, W
E_{Le} – exergy losses by convection and radiation heat transfer from absorber to environment, W
E_{LO} – optical exergy losses, W
$E_{L\Delta T}$ – exergy losses by heat transfer to the working fluid, W
$E_{L\Delta P}$ – exergy losses by friction, W
E_n – net exergy flow, W
E_s – exergy of solar radiation, W
f – friction factor
F_P – plate efficiency factor
F_R – collector heat-removal factor
G – mass velocity of air, kg/s m^2
h – convective heat transfer coefficient, W/m^2 K
h_w – convective heat transfer coefficient due to wind, W/m^2 K
H – duct depth, m
I – solar irradiance, W/m^2
k – thermal conductivity of air, W/m K
k_g – thermal conductivity of glass cover, W/m K
k_i – thermal conductivity of insulation, W/m K
L – length of duct, m
l_g – thickness of glass cover
m – mass flow rate of air, kg/s
N – number of glass covers
p – rib pitch, m
P_m – pumping power, W
ΔP – pressure drop across the duct, Pa
Q_u – useful heat gain, W
t_e – thickness of edge, m
t_i – thickness of edge insulation, m
T_a – ambient temperature, K
T_f – mean air temperature, K
T_g – temperature of glass, K
T_i – air inlet temperature, K
T_o – outlet air temperature, K
T_{pm} – mean plate temperature, K
T_{sky} – sky temperature, K
T_{sun} – sun temperature, K
ΔT – air temperature rise across the duct, K
$\Delta T/I$ – temperature rise parameter, Km^2/W
U_b – bottom loss coefficient, W/m^{2}K
U_L – overall heat loss coefficient, W/m^{2}K
U_s – top loss coefficient, W/m^{2}K
U_t – side loss coefficient, W/m^{2}K
V_w – wind velocity, m/s
W – width of duct, m

Greek symbols

α	–	rib angle of attack, deg
ρ	–	density of air, kg/m^3
σ	–	Stefan-Boltzman's constant, W/m^{2}K^4
μ	–	dynamic viscosity of air, Ns/m^2
δ_i	–	thickness of insulation, m
ε_p	–	emissivity of absorber plate
ε_g	–	emissivity of glass cover
$\tau\alpha$	–	transmittance-absorptance product
η_C	–	Carnot efficiency
η_{th}	–	thermal efficiency
η_e	–	exergetic or exergy efficiency
η_{ex}	–	exergy-to-energy ratio of sun radiation

Dimensionless parameters

e/D_h	–	relative roughness height
f_r	–	friction factor of roughened duct
Nu$_r$	–	Nusselt number of roughened duct
p/e	–	relative roughness pitch
Pr	–	Prandtl number
Re	–	Reynolds number

Abbreviations

SAH	–	solar air heater
THP	–	thermohydraulic performance

1 Introduction

Fossil fuel sources are confined and so the present scenario of energy consumption and growth are not sustainable in the longer term [1]. The energy demand for different applications can be attained by pick up of the solar energy efficiently. Solar energy is the most promising source of energy and the simplest and efficient way of using solar energy is to convert it into thermal energy for heating applications such as space heating, drying of agricultural products and various industrial applications by using solar air heater. The solar air heater is not efficient due to low convective heat transfer coefficient between absorber plate and flowing air. The low rate of heat transfer coefficient is due to presence of a viscous sub-layer. Artificial roughness on the underside of the absorber plate breaks up the laminar sub-layer and increases heat transfer. Increased heat transfer makes the system more effective. Various investigators have investigated the effect of heat transfer and friction factor in various geometries of artificial roughness in a solar air heater duct. The artificial roughness was created on

the wall of the duct single, double and three sides. Prasad and Mullick [2] used artificial roughness in a solar air heater (SAH) in the form of protruding wires to enhance the heat transfer coefficient and plate efficiency factor. Prasad and Saini used small diameter wire on absorber plate and established the effect of relative roughness height and relative roughness pitch of the roughness geometry on the heat transfer and friction factor [3]. Gupta *et al.* [4] investigated effect of relative roughness height and angle of attack on heat transfer and friction factor for inclined circular wire ribs for relative roughness pitch of 10 and 7.5. Saini and Saini investigated expanded metal mesh artificial roughness on the absorber plate of a SAH and obtained considerable enhancement of heat transfer[5]. Verma and Prasad reported maximum enhancement of thermo-hydraulic performance at a roughness Reynolds number of 24 [6]. Karwa *et al.* [7] investigated effect of rib chamfer angle and duct aspect ratio on heat transfer and friction factor using integral chamfered ribs. Chamfer angle of 15° gave highest Stanton number as well as highest friction factor. Bhagoria *et al.* [8] investigated wedge shaped transverse integral rib roughness. Maximum heat transfer occurred for relative roughness pitch of 7.57. Wedge angle of 10° gave maximum enhancement of heat transfer. Momin *et al.* [9] reported V- shape ribs give maximum value of the Nusselt number as compared to inclined ribs. Maximum thermohydraulic performance was attained at an angle of attack 60°. Karwa investigated the effect of transverse, inclined, V continuous and V-discrete pattern ribs on heat transfer enhancement [10]. V pattern ribs were tested pointing upstream and downstream to flow. Based on equal pumping criteria V-down arrangement gave best heat transfer performance. Sahu and Bhagoria reported that at larger pitch value the number of reattachment points becomes less and at low pitch value the number of reattachment point is negligible due to which rate of heat transfer decreases [11]. Jaurker *et al.* [12] investigated the effect of rib-grooved artificial roughness on heat transfer and friction characteristics of solar heater. Thermohydraulic performance of rib-grooved duct was superior as compared to ribbed duct only. Karmare *et al.* [13] investigated the latter effect using metal grit ribs as roughness. Layek *et al.* [14] investigated performance of solar air heater using integral transverse chamfered rib groove roughness. Aharwal *et al.* [15] investigated the inclined rib with gap creating the secondary flow along the rib that joins the main flow to accelerate it and energizes the retarded boundary layer along the surface. This enhances the heat transfer through the gap width area behind the

rib at angle of attack of 60°. Varun *et al.* [16] studied heat transfer and friction characteristics using combination of inclined as well as transverse ribs. Singh *et al.* [17] reported that Nusselt number of V-down discrete rib is better than V-down continuous rib at relative gap position of 0.65. Mittal *et al.* [18] studied the effective efficiency of five different types of roughness elements on the absorber plate and compared with the conventional solar air heater. Layek *et al.* [19] studied numerically the second law optimization of a solar air heater having chamfered rib-groove roughness on absorber plate. It is observed that the entropy generation decreases with increase in relative roughness height. Also the minimum rise in entropy generation at relative roughness pitch of 6, relative groove position 0.4 and chamfer angle 18°.

The researcher [3,4,7] investigated that the dimensionless roughness parameters such as relative roughness pitch, relative roughness height, angle of attack duct aspect ratio, etc., have significant effect on heat transfer and friction characteristics of the rib roughened solar air heater duct.

The artificial roughness used in the path of air passage in SAH to enhancement technique of heat transfer rate by which thermohydraulic performance of a SAH can be improved but friction loss also increases simultaneously due to presence of roughness elements which requires more power of blower or pump to drive the air through the duct. It is important to know the roughness element geometry and its parameters combination which will deliver higher thermal performance and low friction factor of a solar air heater. So to improve the overall performance of the solar air heater requires minimizing the undesirable power consumption of blower or pump. The objectives of high heat transfer rates and low friction losses can be executed when the design of the flow duct and absorber surface of solar air heaters consider the balance between useful energy and friction losses in the light of the second law considerations. It defines the net exergy flow as a suitable quantity for the optimization of solar air heaters having different design and roughness elements. The exergy is the maximum work potential that can be obtained from a form of energy [20]. Exergy analysis, derived from both the first and second laws of thermodynamics, as compared to energy analysis, takes into account the quality of the energy transferred. Exergy analysis is a powerful tool for design, optimization, and performance evaluation of solar thermal utilization systems [21–24].

Kurtbas and Durmus studied the exergy loss of the system decreases depending on the increase of the collector efficiency [25]. There is a reverse

relationship between dimensionless exergy loss and heat transfer, as well as pressure loss. Ozturk studied the energy and exergy efficiencies of the solar parabolic cooker [26]. The energy efficiencies are relatively very low, in particular the exergy efficiency. It is applied to all devices utilizing the solar radiation. Gupta and Kaushik parametrically studied the maximum exergy delivery during the collection of solar energy in a smooth solar air heater [27]. They studied six roughness geometries in the absorber plate of solar air heater duct in terms of energy, effectiveness and exergy efficiencies[28]. Moreover they parametrically studied the expanded metal mesh roughness geometries in the absorber plate of solar air heater duct in terms of energy augmentation ratio, effective energy augmentation ratio and exergy augmentation ratio [29]. Another study [30,31] relates to a new flat-plate solar air heater with three types of obstacles in terms of first and second law efficiencies. Pandey *et al.* [32] studied two different types of solar cookers based on the exergy analysis. Benli investigated five types of air heating solar collectors in terms of collector efficiencies, friction coefficient and exergy loss [33]. The performance of solar collector has been examined from the standpoint of energy balance approach. It is important to note that this approach gives a very poor indication of how well a particular energy resource is being utilized by a system to accomplish a specific objective. Thus it has been necessary to resort to the second law of thermodynamics for evaluation of solar system. The second law efficiency or exergy efficiency address the quality of energy [22].

In this study, W-shaped roughness geometry suggested by Lanjewar *et al.* [34], as shown in Fig. 1 has been considered for the absorber surface of the roughened duct SAH because the experimental analysis has shown the thermohydraulic performance (THP) advantage of such roughness in a uniform heated duct whose thermal boundary condition correspond closely to those found in SAH. A detailed investigation has been carried out using a mathematical model to study the effect of a system and operating parameters on the thermal and exergy efficiency. The correlation of the Nusselt number and friction factor obtained from experimentation has been used to carry out numerical analysis. The results obtained for the SAH with W-shaped roughened surface have also been compared with those of the conventional flat-plate SAH under same operating conditions.

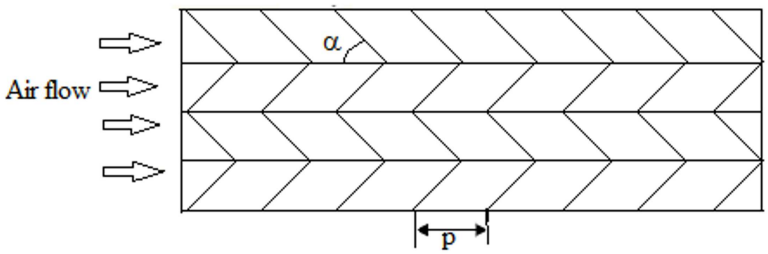

Figure 1: W-shape rib arrangement.

2 Energy and exergy analysis of flat plate solar air heater

2.1 Energy analysis

The thermal efficiency of the solar air heater defined as the ratio of the useful energy gain over some specified time period to the incident solar energy over the same time period [35]. The thermal efficiency of the solar air heater is given by

$$\eta_{th} = \frac{Q_u}{IA_c} = mC_p \frac{(T_o - T_i)}{IA_c} \ , \tag{1}$$

where Q_u is the useful heat gain, I is the solar irradiance, A_c is the surface area of absorber plate, m is the mass flow rate of air, C_p is the specific heat of air, T_0 and T_i are the outlet and inlet air temperature, respectively.

2.2 Exergy analysis

Exergy has the same dimension as energy, it can be compared directly to pumping power, and a new criterion can be established and suggests a criterion for optimum control and performance evaluation of solar thermal systems including solar air heater [21]. The net exergy flow represent the increase of the exergy flow of the air, during the time that passing through the collector, is maximized for optimization. Neglecting changes of kinetic and potential energy and treating air as a perfect gas [36], the net exergy flow can be expressed by

$$E_n = IA_c\eta_{th}\eta_C - P_m\left(1 - \eta_C\right) \ , \tag{2}$$

where P_m is the pump work and η_C is the Carnot efficiency. The first term on the right hand side of Eq. (2) represents the exergy of the absorber solar energy transferred to the air and the second term represents the exergy losses due to friction.

The Carnot efficiency is evaluated by the formulae:

$$\eta_C = \left(1 - \frac{T_a}{T_f}\right) , \tag{3}$$

where T_a is the ambient temperature. The mean air temperature is the simple arithmetic mean of the measured temperature values at the inlet and the exit of the test section

$$T_f = \frac{T_i + T_o}{2} . \tag{4}$$

The exergy of solar radiation is defined as the context of measurements of the global radiation balance [37]

$$E_s = IA_c\eta_{ex} = IA_c\left(1 - \frac{T_a}{T_{sun}}\right) . \tag{5}$$

Patela demonstrated that sun temperature (T_{sun}) is approximately 3/4 of the apparent black-body temperature of the sun (T_{sun} = 6000 K) [38]. Exergy-to-energy ratio of sun radiation is given by the relation

$$\eta_{ex} = \left(1 - \frac{T_a}{T_{sun}}\right) .$$

The exergetic efficiency is defined as

$$\eta_e = \frac{E_n}{E_s} . \tag{6}$$

The exergetic efficiency can be maximized by maximizing the net exergy flow and minimizing exergy losses by absorption of radiation. The various components of exergy losses are [36]:

I. Optical exergy losses

$$E_{Lo} = IA_c\eta_{ex}\left(1 - \tau\alpha\right) , \tag{7}$$

where $\tau\alpha$ is the transmittance-absorptance product.

II. Exergy losses due to absorption of irradiation by the absorber

$$E_{LA} = IA_c(\tau\alpha)\left[\eta_{ex} - \left(1 - \frac{T_a}{T_{pm}}\right)\right], \tag{8}$$

where T_{pm} is the mean plate temperature.

III. Exergy losses by heat transfer to environment

$$E_{Le} = U_L A_c (T_{pm} - T_a)\left(1 - \frac{T_a}{T_{pm}}\right), \tag{9}$$

where U_L is the overall heat loss coefficient.

IV. Exergy losses by heat transfer to the working fluid

$$E_{L\Delta T} = IA_c\eta_{th}\left(\frac{T_a}{T_f} - \frac{T_a}{T_{pm}}\right). \tag{10}$$

V. Exergy losses by friction

$$E_{L\Delta P} = m(\Delta P)\left(\frac{T_a}{\rho T_f}\right), \tag{11}$$

where ΔP is the pressure drop, and ρ is density of air.

The most important exergy loss results from the absorption of irradiation by the absorber at the mean plate temperature. A high absorber temperature decreases the exergy losses by absorption but also increases the thermal losses (E_{Le}) to the environment.

3 Mathematical model

An important characteristic of solar air heater of thermal behaviour is the flow path of air. The thermal behaviour of SAH with rib roughened absorber plate is similar to that of conventional flat- plate SAH. The same procedure of the conventional SAH use the calculating absorbed irradiation and the heat losses for roughened SAH. The following assumptions are made:

- steady state conditions,

- negligible heat conduction in flow direction,
- negligible edge effects,
- constant air flow throughout the SAH.

The experimental investigations to determine the Nusselt number and friction factor of the W- shaped rib roughened duct depending on geometrical parameters have been done by the authors [34]. Correlations are used here for the numerical analysis. The objective of this work is to present a methodology for optimum design of SAH and the results need to be presented as function of basic design parameters, namely: temperature rise parameter ($\Delta T/I$), solar irradiation (I), and Reynolds number (Re). Solar irradiation is an incident solar radiation. It is a measure of the solar energy incident on a given area over a specific period of time. The salient features of the procedure followed for determination of exergetic efficiency of SAH and stepwise calculation procedure is given below [39,40]:

Step 1 Selection of the system and operating parameters: the range of system parameters including roughness geometry [34] and operating parameters, as given in Tab. 1, for the collector under consideration, have been selected.

Step 2 In the present study it is considered that the ambient air is sucked into the SAH duct, so the inlet air temperature (T_i) is taken equal to the ambient temperature (T_a). The outlet air temperature (T_o) be calculated from given temperature rise of air across the duct (ΔT) and the inlet air temperature

$$T_o = \Delta T + T_i \, . \tag{12}$$

Step 3 To start the calculation process of useful heat gain, i.e., the rate of heat transfer to the working fluid, initialize the mean plate temperature.

Step 4 Calculation of overall heat loss coefficient (U_L), which is the sum of the top heat loss coefficient (U_t), bottom loss coefficient (U_b), and side loss coefficient (U_s)

$$U_L = U_t + U_b + U_s \, . \tag{13}$$

The bottom heat loss coefficient is calculated using the relation

$$U_b = \frac{k_i}{\delta_b} \, , \tag{14}$$

where k_i is the thermal conductivity of insulation and δ_i is the thickness of insulation. The side heat loss coefficient is calculated using the relation

$$Us = \frac{(L+W)\, t_e k_i}{LW t_i} \ , \tag{15}$$

where L and W are the length and width of the duct, t_e is the thickness of edge, and t_i is the thickness of edge insulation. The top heat loss coefficient is a function of number of parameters such as mean absorber plate temperature, ambient temperature, etc., is computed using the relationship proposed by Klein [41]

$$U_t = \left[\frac{N}{\left(\frac{C}{T_{pm}}\right)\left[\frac{T_{pm}-T_a}{N+f}\right]^{et}} + \frac{1}{h_w} \right]^{-1} + \frac{\sigma\left(T_{pm}^2 + T_a^2\right)\left(T_{pm}+T_a\right)}{\left(\varepsilon_p + 0.00591 N h_w\right)^{-1} + \left[\frac{(2N+f-1)+0.133\varepsilon_p}{\varepsilon_g}\right] - N}, \tag{16}$$

where N is the number of glass covers, ϵ_p and ϵ_g are the the emissivity of absorber plate and of glass cover, respectively. Here:

$$f = \left(1 + 0.089 h_w - 0.1166 h_w \varepsilon_p\right)\left(1 + 0.07866 N\right) \ , \tag{17}$$

$$et = 0.43\left(1 - \frac{100}{T_{pm}}\right) \ , \tag{18}$$

$$C = 520\left(1 - 0.000051\beta^2\right) \ , \tag{19}$$

where β is the heater tilt angle. The convective heat transfer coefficient for air flowing over the outside surface of the glass cover is proposed by McAdams [42] as follows:

$$h_w = 5.7 + 3.8 V_w \ , \tag{20}$$

where V_w is the wind velocity.

From the outer surface of the glass cover at temperature (T_{go}), the heat is lost by radiation to the sky temperature (T_{sky}) and by convection to the ambient air, hence [43]

$$Q_{tgo} = A_c\left[h_r\left(T_{go} - T_{sky}\right) + h_w\left(T_{go} - T_a\right)\right] \ , \tag{21}$$

where h_r is the radiation heat transfer coefficient

$$h_r = \sigma \varepsilon_g \left(T_{go}^2 + T_{sky}^2\right)\left(T_{go} + T_{sky}\right) \ . \tag{22}$$

The sky temperature is calculated using the Swinbank [44] relation

$$T_{sky} = 0.0552 T_a^{1.5} \ . \tag{23}$$

Step 5 Calculation of useful heat gain rate using the following relation:

$$Q_{u1} = A_c \left[I\tau\alpha - U_L \left(T_{pm} - T_a\right)\right] \ . \tag{24}$$

Step 6 Calculation of mass flow rate of air (m), mass velocity (G) and the flow Reynolds number (Re) are determined as:

$$m = \frac{Q_{ul}}{C_p \Delta T} \ , \tag{25}$$

$$G = \frac{m}{WH} \ , \tag{26}$$

$$\mathrm{Re} = \frac{G D_h}{\mu} \ , \tag{27}$$

where H and W are the depth and width of duct, D_h is the hydraulic diameter of duct, and μ is the dynamic viscosity of air.

The Nusselt number is first calculated from the correlation developed on the basis of experimental result for W-shaped rib by Lanjewar *et al.* [34]

$$\mathrm{Nu}_r = 0.0613 \mathrm{Re}^{0.9079} \left(\frac{e}{D_h}\right) 0.4487 \left(\frac{\alpha}{60}\right)^{-0.1331} \times \left\{\exp\left[-0.5307 \left(\ln\left(\frac{\alpha}{60}\right)\right)^2\right]\right\} \ , \tag{28}$$

where e is the rib height, α is the angle of attack and e/D_h denotes the relative roughness. The average absolute deviation in the predicted values of Nusselt number was 5.23% whereas the regression coefficient is 0.92 and Nusselt number lies within ±11% deviation lines of the experimental values of Nusselt number [34].

Step 7 The plate efficiency factor (F_P) and heat transfer coefficient (h) are determined using the relations as:

$$F_p = \frac{h}{h + U_L}\,, \tag{29}$$

$$h = \frac{k\mathrm{Nu}}{D_h}\,. \tag{30}$$

Step 8 The collector heat-removal factor is calculated as

$$F_R = \frac{mC_p}{U_L A_c}\left\{1 - \exp\left[-\frac{F_p U_L A_c}{mC_p}\right]\right\}. \tag{31}$$

Step 9 The useful heat gain rate is calculated from the heat removal factor as

$$Q_{u2} = F_R A_c \left[I\tau\alpha - U_L\left(T_o - T_a\right)\right]. \tag{32}$$

Step 10 Check if the two values of useful heat gain rate calculated as Q_{u1} in Eq. (24) and Q_{u2} in Eq. (32), are close enough which the iterations are done, a new value of mean plate temperature is calculated

$$T_{pm} = T_a + \frac{[I\tau\alpha - Q_{u2}/A_c]}{U_L}. \tag{33}$$

Step 11 The thermal efficiency is calculated from the useful heat gain rate Q_u, which is the average of Q_{u1} and Q_{u2}, as

$$\eta_{th} = \frac{Q_u}{IA_c}. \tag{34}$$

Step 12 The friction factor is first calculated from the correlation developed on the basis of experimental result for W-shaped rib by Lanjewar *et al.* [34]

$$f_r = 0.6182\mathrm{Re}^{-0.2254}\left(\frac{e}{D_h}\right)^{0.4622}\left(\frac{\alpha}{60}\right)^{0.0817} \times\left\{\exp\left[-0.28\left(\ln\left(\frac{\alpha}{60}\right)\right)^2\right]\right\}. \tag{35}$$

The average absolute deviation in the predicted values of friction factor was 0.01%, whereas the regression coefficient is 0.93, and the friction factor lying within ±5% of deviation lines of the experimental values of friction factor [34].

Step 13 The pressure drop across the duct is calculated as

$$\Delta P = \frac{2 f_r L V^2 \rho}{D_h} , \tag{36}$$

where V is the air velocity.

Step 14 The pump work is required to drive air through the collector is calculated as

$$P_m = \frac{m \Delta P}{\rho} . \tag{37}$$

Step 15 The exergetic efficiency is calculated from Eq. (6). The calculations are repeated for next set of roughness parameters, temperature rise parameter and solar irradiance to cover the entire range of values as given in Tab. 1.

Table 1: System and operating parameters used in this present study.

Description	Parameter	Units	Values
System parameter			
Collector length	L	m	1.5
Collector width	W	m	0.2
Heater tilt angle	β	deg	0
Duct depth	H	m	0.025
Number of glass cover	N		1
Thermal conductivity of insulation	K_i	W/mK	0.037
Thickness of insulation	d_i	m	0.05
Transmittance-absorptance product	$\tau\alpha$		0.80
Emissivity of absorber plate	ε_p		0.90
Emissivity of glass cover	ε_g		0.88
Relative roughness pitch	p/e		10
Angle of attack	α	deg	30–75
Relative roughness height	e/D_h		0.0180–0.03375
Operating parameters			
Ambient temperature	T_a	K	300
Wind velocity	V_w	m/s	1
Temperature rise parameter	$\Delta T/I$	Km^2/W	0.004–0.030
Solar irradiance	I	W/m^2	500–1000

4 Results and discussion

The exergetic efficiency is calculated numerically using the above approach for different roughness parameters of the W-shaped rib roughened solar air heater at various temperature rise parameter ($\Delta T/I$) and solar irradiance (I) as listed in Tab. 1.

Figure 2 indicated that the variation of thermal efficiency and exergetic efficiency as a function of Reynolds number for the value of rib roughness parameters of $p/e = 10$, $e/D_h = 0.03375$ and $\alpha = 60°$. It is observed that the thermal efficiency increase with increase in the Reynolds number. It is due to the fact that the increase in Reynolds number causes the increase in heat transfer coefficient from the absorber plate to air. The exergetic efficiency increases with the increase in Reynolds number up to 2350 and after attaining maximum it starts decreasing with further increase in the Reynolds number. It happens due to higher exergy losses at higher Reynolds number. With increase of mass flow rate of air and resulting increase in Reynolds number, the exergy associated with the required pump work exceeds exergy of thermal energy collected and thus the net exergy flow and thereby the exergetic efficiency becomes negative.

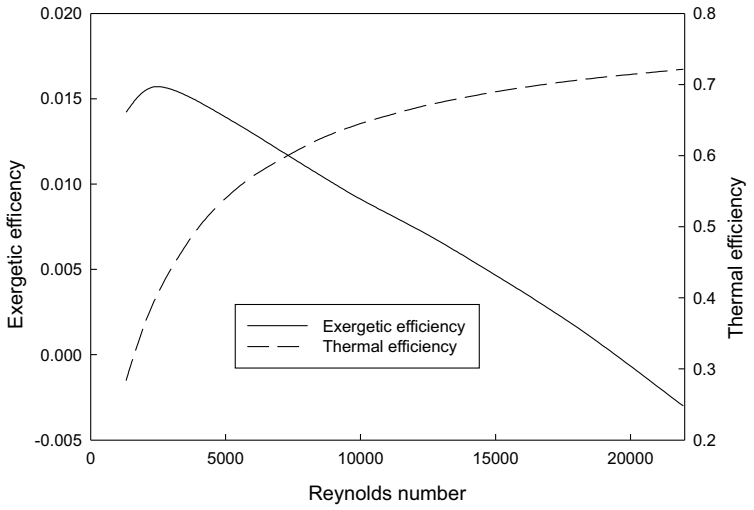

Figure 2: Variation of thermal efficiency and exergetic efficiency with Reynolds number for W-shaped rib roughened solar air heater having rib-roughness parameters as $p/e = 10$, $e/D_h = 0.03375$ and $\alpha = 60°$ at solar irradiance of 1000 W/m^2.

Figure 3 indicated the variation of thermal efficiency and exergetic efficiency as a function of temperature rise parameter for the value of rib roughness parameters of p/e =10, e/D_h = 0.03375 and $\alpha = 60°$. It is observed that the thermal efficiency decreases with increase in the temperature rise parameter. The exergetic efficiency increase with increases in the temperature rise parameter up to 0.02355 K m^2/W, and then it starts decreasing with further increase in the temperature rise parameter.

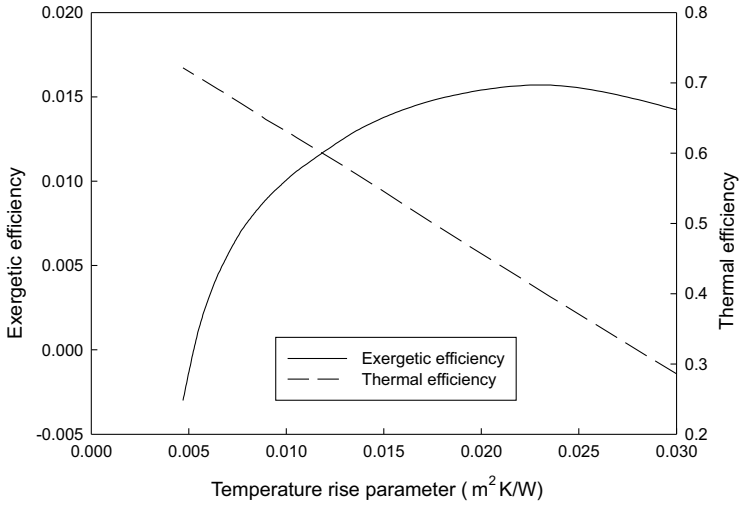

Figure 3: Variation of thermal efficiency and exergetic efficiency with temperature rise parameter for W-shaped rib roughened solar air heater having rib-roughness parameters as p/e = 10, e/D_h = 0.03375 and $\alpha = 60°$ at solar irradiance of 1000 W/m^2.

Figure 4 indicated that the variation in exergetic efficiency with the Reynolds number can be explained by taking into consideration the exergy losses components. It is observed that the optical losses (E_{LO}) remain independent of the Reynolds number. The most essential exergy loss (E_{LA}) results from the absorption of irradiation by the absorber at the mean temperature. High absorber temperature decreases the exergy losses by absorption but increases the thermal losses (E_{Le}) to the environment. Figure shows that the exergy losses to the environment decrease with increase in Reynolds number. It is due to the fact that the absorber plate temperature decreases with increases of the Reynolds number causes the decrease of exergy losses to environment. The exergy losses by heat transfer to air ($E_{L\Delta T}$ and the

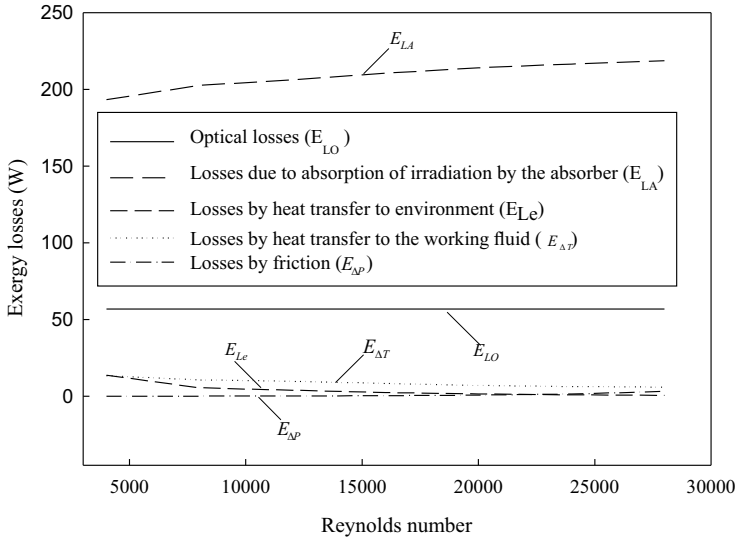

(a)

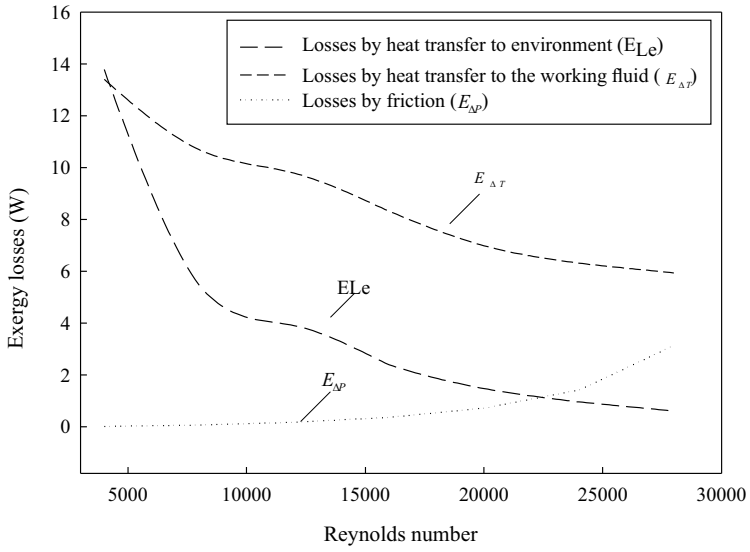

(b)

Figure 4: (a) Variation of exergy losses components with Reynolds number for W-shaped rib roughened solar air heater having rib-roughness parameters as $p/e = 10$, $e/D_h = 0.03375$ and $\alpha = 60^\circ$ at solar irradiance (I) of 1000 W/m^2. (b) Expanded view of exergy loss components.

exergy losses by friction ($E_{L\alpha\Delta P}$) result from internal irreversibilities, heat transfer from the absorber plate to air at finite temperature difference and friction in the flow SAH duct. Figure 4(b) shows clearly the expanded view of the effect of the Reynolds number on these exergy components. The exergy losses by heat transfer to air decrease and the exergy losses by friction increase with increasing Reynolds number. The decrease in ($E_{L\Delta T}$ may be attributed to decrease in the absorber plate temperature and decrease of temperature difference between inlet and outlet with increase in the Reynolds number. At lower Reynolds number the exergy losses by heat transfer to air are high. It is observed in Fig. 4(b) that at higher Reynolds number increases the turbulent flow intensity, pumping work and the irreversibility, so exergy loss by friction goes on increasing with increase in the Reynolds number.

Figures 5–8 shown the variation in exergetic efficiency (η_e) as a function of Reynolds number (Re) and temperature rise parameter ($\Delta T/I$) at different relative roughness height (e/D_h) and the angle of attack (α) for constant solar irradiance (I) and other geometrical parameters.

4.1 Effect of different relative roughness height

Figure 5 indicated the value of exergetic efficiency as a function of Reynolds number for different relative roughness heights. The highest exergetic efficiency obtained at relative roughness height $e/D_h = 0.03375$ for $\mathrm{Re} < 12\,500$, however for $\mathrm{Re} > 18\,000$ the smooth plate solar air heater gives the highest exergetic efficiency. It is also observed that for the Reynolds number in the range of 12 500–18 000 different values of relative roughness height return the highest value of exergetic efficiency.

Figure 6 indicated the value of exergetic efficiency as a function of temperature rise parameter for different relative roughness height. It is observed that relative roughness height $e/D_h = 0.03375$ shows the highest values of exergetic efficiency for $\Delta T/I > 0.0089$ Km^2/W as compared to other relative roughness height values. Smooth conventional solar air heater gives the highest exergetic efficiency for $\Delta T/I < 0.0055$ Km^2/W as compared to roughened solar air heater duct.

4.2 Effect of different angle of attack

Figure 7 indicated the value of exergetic efficiency as a function of Reynolds number for different angles of attack. It is observed that the highest ex-

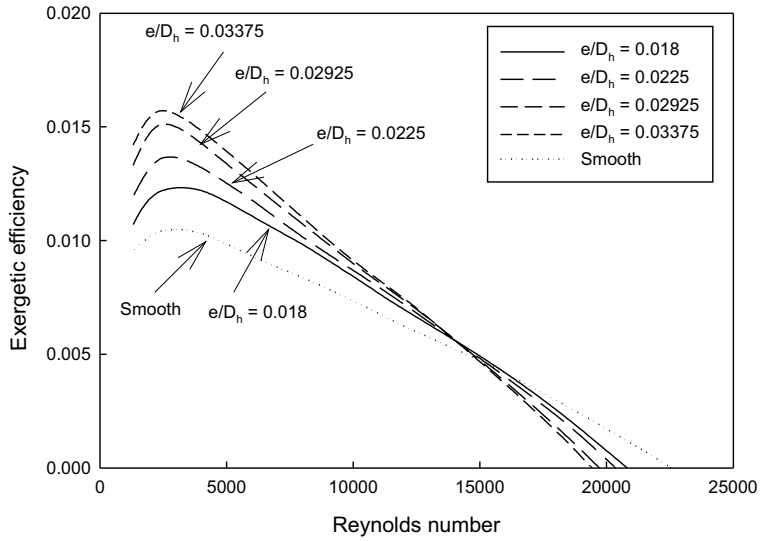

Figure 5: Exergetic efficiency as a function of Reynolds number for different relative roughness heights for $p/e = 10$, $\alpha = 60^\circ$, $I = 1000$ W/m^2.

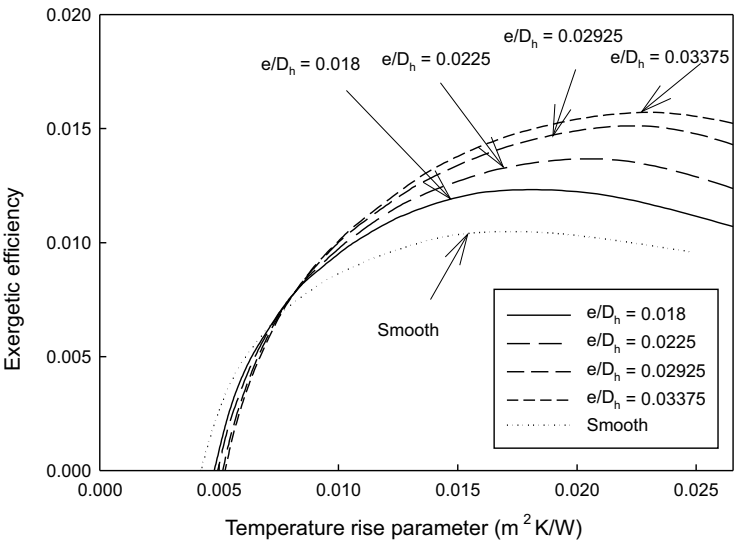

Figure 6: Exergetic efficiency as a function of temperature rise parameters for different relative roughness heights for $p/e = 10$, $\alpha = 60^\circ$, $I = 1000$ W/m^2.

ergetic efficiency obtained at an angle of attack $\alpha = 60°$ for Re < 8000, however for Re $> 18\,000$ the smooth plate solar air heater gives highest exergetic efficiency. It is also observed that for Reynolds number in range of 8000–18 000 different value of angle of attack gives the highest values of exergetic efficiency.

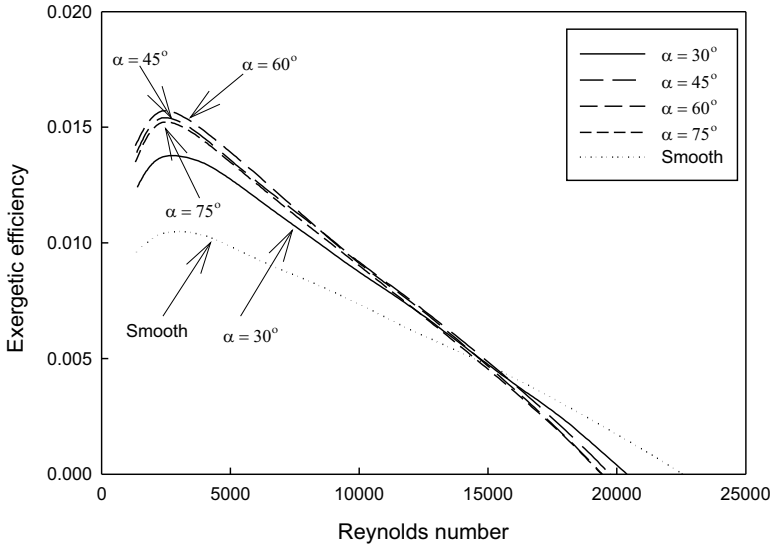

Figure 7: Exergetic efficiency as a function of Reynolds number for different angle of attack for $p/e = 10$, $\alpha = 60°$, $I = 1000$ W/m^2.

Figure 8 indicated the value of exergetic efficiency as a function of temperature rise parameter for different angles of attack. It is observed that the angle of attack $\alpha = 60°$ shows the highest values of exergetic efficiency for $\Delta T/I > 0.0105$ m^{2}K/W as compared to other angles of attack. Smooth conventional solar air heater gives the highest exergetic efficiency for $\Delta T/I < 0.0059$ m^{2}K/W as compared to roughened solar air heater duct.

From the above discussion, it is observed that no particular value of roughness parameter obtained maximum exergetic efficiency in the investigated range of the Reynolds number and temperature rise parameter. It is observed from Figs. 5 and 7 that exergetic efficiency increases with increase in Reynolds number. Following attained maximum at certain Reynolds number, it starts decreasing with further increasing in Reynolds number.

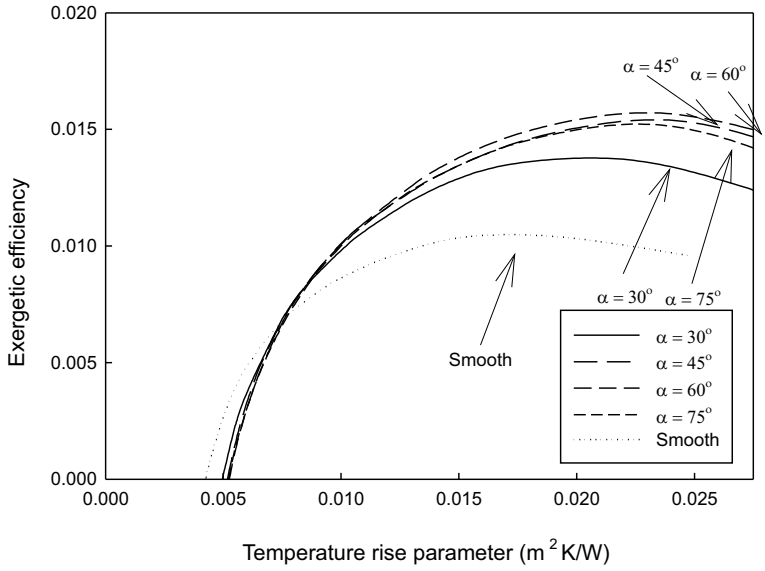

Figure 8: Exergetic efficiency as a function of temperature rise parameters for different angles of attack for $p/e = 10$, $\alpha = 60°$, $I = 1000$ W/m^2.

It is seen that the exergetic efficiency of smooth plate solar air heater is higher as compared to roughened solar air heater at higher Reynolds number. It is due to the fact that the higher Reynolds number causes the increase in exergy losses by friction of the roughened solar air heater as compared to that of the smooth plate solar air heater. At higher Reynolds number the useful heat gain is lower as compared to the pumping power. Figures 6 and 8 show that exergetic efficiency increases with increase of the temperature rise parameter. After attained maximum at certain $\Delta T/I$, it starts decreasing with further increasing of $\Delta T/I$. It is seen that the exergetic efficiency of smooth plate solar air heater is higher as compared to the roughened solar air heater at lower range of temperature rise parameter ($\Delta T/I < 0.0059$ m^{2}K/W). It is observed that the maximum enhancement in exergetic efficiency of W-shaped rib roughened solar air heater as compared to smooth plate solar air heater has been obtained as 51% corresponding to $e/D_h = 0.03375$ and $\alpha = 60°$.

4.3 Optimization of roughness geometry parameters

Figures 9 and 10 shows optimum values of relative roughness height (e/D_h) and angle of attack (α) that correspond to maximum exergetic efficiency for a given value of temperature rise parameters ($\Delta T/I$) at different solar irradiance.

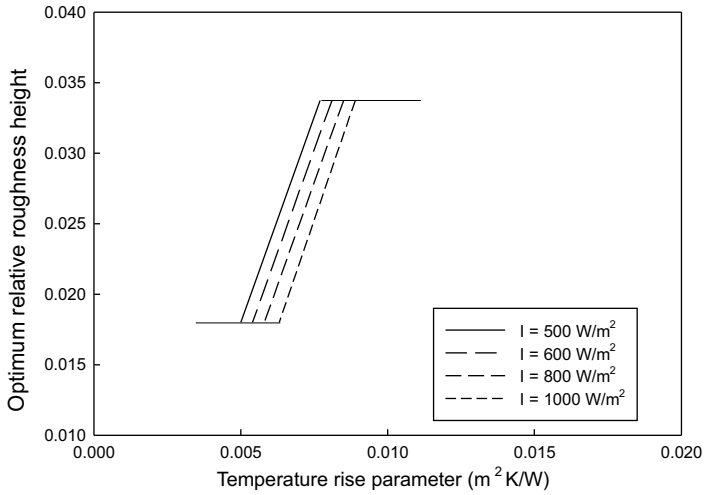

Figure 9: Optimum values of relative roughness height on the basis of exergetic efficiency.

Figure 9 shows the plot of the relative roughness height versus temperature rise parameters at different solar irradiances. From figure it is seen that for all values of solar irradiance the relative roughness height of 0.03375 is optimal for $\Delta T/I > 0.0089$ ^{2}Km/W, whereas the relative roughness height of 0.018 is the optimum for $\Delta T/I < 0.0050$ m^{2}K/W. For $\Delta T/I$ in the range of 0.0050–0.0089 m^{2}K/W, the optimum relative roughness height is a function of temperature rise parameter for different value of solar irradiance.

Figure 10 shows the plot of the angle of attack versus temperature rise parameters at different solar irradiance. From figure it is seen that for all values of solar irradiance the angle of attack of 60° is optimum for $\Delta T/I > 0.0105$ m^{2}K/W, whereas the angle of attack of 30° is optimum for $\Delta T/I < 0.0045$ m^{2}K/W. For $\Delta T/I$ in the range of 0.0045–0.0105 m^{2}K/W, the optimum angle of attack is a function of temperature rise parameter for different values of solar irradiance.

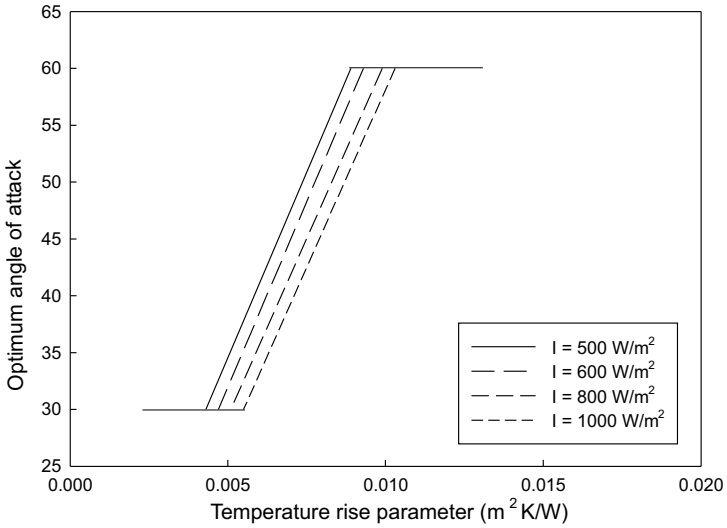

Figure 10: Optimum values of angle of attack on the basis of exergetic efficiency.

4.4 Comparison of exergetic efficiency of roughened solar air heater

Figure 11 indicated that the comparison of exergetic efficiency of W-shaped rib roughness with two other roughness geometries which are transverse wire and inclined continuous rib for the value of rib roughness parameters of relative roughness pitch $p/e = 10$, relative roughness height $e/D_h = 0.03375$, angle of attack $\alpha = 60°$ and solar irradiance $I = 1000$ W/m^2. It is observed that the exergetic efficiency of W-shaped rib roughness becomes greater than exergetic efficiency of transverse wire and inclined continuous ribs for all values of Reynolds number. In the casee where the Reynolds number is greater than 18 000 the exergy efficiency is negative for W-shaped, transverse wire and inclined continuous ribs, because of increase in Reynolds number, the exergy associated with the required pump work exceeds the exergy of thermal energy collected and thus the net exergy flow and thereby the exergetic efficiency becomes negative.

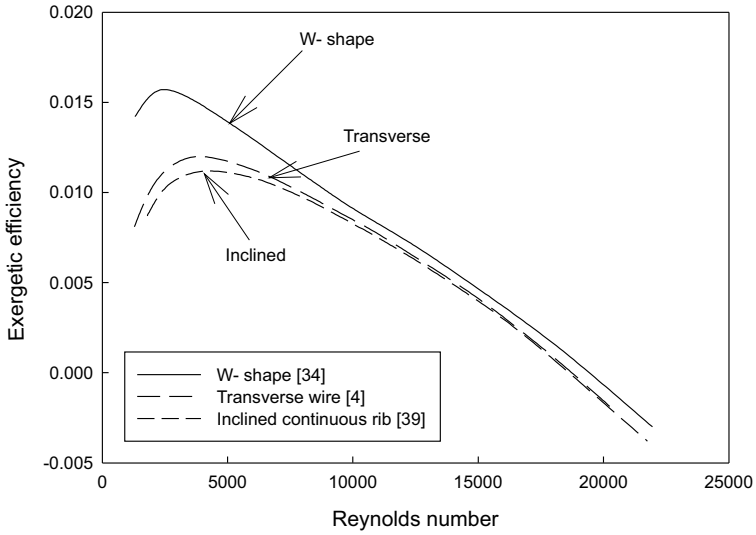

Figure 11: Comparison of exergetic efficiency of W-shaped rib roughness and other roughness geometries of roughened solar air heater for $p/e = 10$, $e/D_h = 0.03375$, $\alpha = 60^\circ$, $I = 1000$ W/m^2.

5 Experimental set-up and validation of mathematical model

The experimental set-up used in the present study has been developed by Lanjewar *et al.* [34]. The mathematical model has been validated in terms of the value of thermal efficiency obtained from mathematical model for smooth surface with the experimental value of thermal efficiency obtained from experimentation.

Figure 12 indicated the thermal efficiency values predicted by the mathematical model plotted with experimental result for smooth plate solar air heater. The average absolute deviation between predicted and experimental values is within $\pm 12\%$. Reasonably good agreement between the experimental and predicted values ensures the accuracy of the mathematical model.

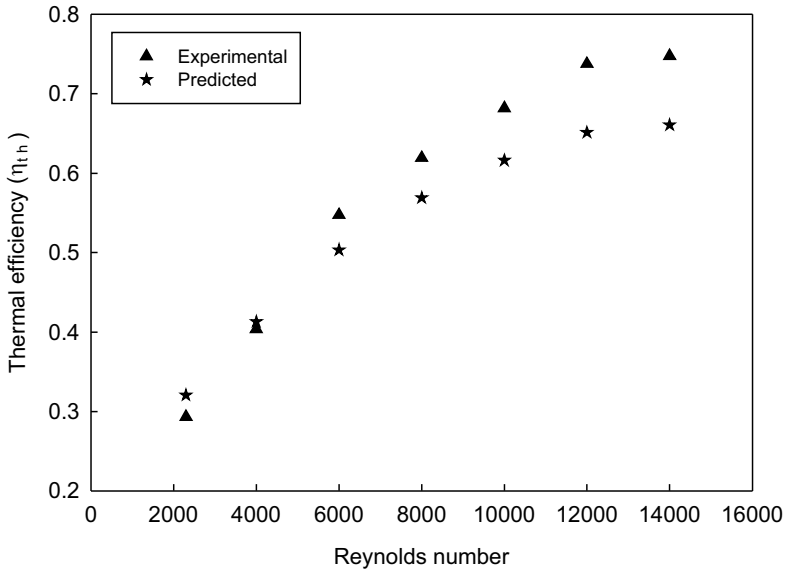

Figure 12: Comparison of experimental and predicted values of thermal efficiency for smooth duct solar air heater.

6 Conclusion

The study presents a mathematical model for predicting the performance of W-shaped roughened solar air heater on the basis of exergetic efficiency and the result obtained have been compared with conventional smooth duct solar air heater under the similar operating conditions. Based on the results the following conclusions are drawn as under:

1. Compared conventional smooth duct solar air heater to W-shaped roughened solar air heater significantly enhanced the exergetic efficiency. The obtained is enhancement in exergetic efficiency 51%.
2. Exergetic efficiency analysis of W-shaped roughness on the basis of Reynolds number, temperature rise parameter and rib roughness parameters has been accomplished. The maximum value of exergetic efficiency of W-shaped roughened solar air heater is obtained for Reynolds number less than 18 000. On increasing the Reynolds number beyond 18 000 the conventional smooth duct solar air heater gives better performance. It is suitable to operate the solar air heater within this range of Reynolds number. At higher Reynolds number

the exergetic efficiency of roughened solar air heater is negative so it is not suitable to run solar air heater beyond this Reynolds number. A set of W-shaped roughened solar air heater roughness parameters namely relative roughness pitch of 10, relative roughness height of 0.03375, angle of attack of 60° and solar irradiance of 1000 W/m^2.

Received 20 February 2018

References

[1] Twidell J., Weir T.: *Renewable Energy Sources*. Taylor & Francis e-Library, 2006.

[2] Prasad K, Mullick S.C.: *Heat transfer characteristics of a solar air heater used for drying purposes*. Appl. Energy **13**(1983), 2, 83–93.

[3] Prasad B.N., Saini J.S.: *Effect of artificial roughness on heat transfer and friction factor in a solar air heater*. Sol. Energy **41**(1988), 6, 555–560.

[4] Gupta D, Solanki S.C., Saini J.S.: *Heat and fluid flow in rectangular solar air heater ducts having transverse rib roughness on absorber plates*. Sol. Energy **51**(1993); 1, 31–37.

[5] Saini R.P., Saini J.S.: *Heat transfer and friction factor correlations for artificially roughened ducts with expanded metal mesh as roughness element*. Int. J. Heat Mass Tran. **40**(1997), 4, 973–986.

[6] Verma S.K., Prasad B.N.: *Investigation for the optimal thermohydraulic performance of artificially roughened solar air heaters*. Renew. Energ. **20**(2000), 1, 19–36.

[7] Karwa R., Solanki S.C., Saini J.S.: *Heat transfer coefficient and friction factor correlations for the transitional flow regime in rib-roughened rectangular ducts*. Int. J. Heat Mass Tran. **42**(1999); 9, 1597–1615.

[8] Bhagoria J.L., Saini J.S., Solanki S.C.: *Heat transfer coefficient and friction factor correlations for rectangular solar air heater duct having transverse wedge shaped rib roughness on the absorber plate*. Renew. Energ. **25**(2002), 3, 341–369.

[9] Momin A.M., Saini J.S., Solanki S.C.: *Heat transfer and friction in solar air heater duct with V-shaped rib roughness on absorber plate*. Int. J. Heat Mass Tran. **45**(2002), 16, 3383–3396.

[10] Karwa R.: *Experimental studies of augmented heat transfer and friction in asymmetrically heated rectangular ducts with ribs on the heated wall in transverse, inclined, V-continuous and V-discrete pattern*. Int. Comm. Heat Mass Tran. **30**(2003), 2, 241–250.

[11] Sahu M.M., Bhagoria J.L.: *Augmentation of heat transfer coefficient by using 90 broken transverse ribs on absorber plate of solar air heater*. Renew. Energy **30**(2005), 13, 2057–2073.

[12] Jaurker A.R., Saini J.S., Gandhi B.K.: *Heat transfer and friction characteristics of rectangular solar air heater duct using rig-grooved artificial roughness*. Solar Energy **80**(2006), 8, 895–907.

[13] Karmare S.V., Tikekar A.N.: *Heat transfer and friction factor correlation forartificially roughened duct with metal grit ribs*. Int. J. Heat Mass Tran. **50**(2007), 21-22, 4342–4351.

[14] Layek A., Saini J.S., Solanki S.C.: *Heat transfer and friction characteristics for artificially roughened ducts with compound turbulators*. Int. J. Heat Mass Tran. **50**(2007), 23-24, 4845–4854.

[15] Aharwal K.R., Gandhi B.K., Saini J.S.: *Experimental investigation on heat transfer enhancement due to a gap in an inclined continuous rib arrangement in a rectangular duct of solar air heater*. Renew. Energ. **33**(2008), 4, 585–596.

[16] Varun, Saini R.P., Singal S.K.: *Investigation of thermal performance of solar air heater having roughness elements as a combination of inclined and transverse ribs on the absorber plate*. Renew. Energ. **33**(2008), 6, 1398–1405.

[17] Singh S., Chander S., Saini J.S.: *Heat transfer and friction factor of discrete V-down rib roughened solar air heater ducts*. J. Renew. Sustain. Ener. **3**(2011), 1, 013108-1–17 .

[18] Mittal M.K., Saini R.P., Varun, Singal S.K.: *Effective efficiency of solar air heaters having different types of roughness elements on the absorber plate*. Energy **32**(2007), 739–745.

[19] Layek A., Saini J.S., Solanki S.C.: *Second law optimization of a solar air heater having chamfered rib-groove roughness on absorber plate*. Renew. Energ. **32**(2007), 1967–1980.

[20] Bejan A.: *Advanced Engineering Thermodynamics*. Wiley Interscience, 1988.

[21] Fujiwara M.: *Exergy analysis for the performance of solar collectors*. J. Sol. Energy Eng. **105**(1983), 163–167.

[22] Said S.A.M., Zubair S.M.: *On second-law efficiency of solar collectors*. J. Sol. Eng. **115**(1993), 1, 2–4.

[23] Binark A.K.: *Exergy analysis for the solar air collectors*. In: Proc. Int. Conf. on Efficiency, Costs, Optimization, Simulation and Environmental Impact of Energy Systems, Istanbul, 11–14, July 1995, 539–544.

[24] Rosen M.A.: *Second law analysis: approaches and implications*. Int. J. Energ. Res. **23**(1999), 5, 415–429.

[25] Kurtbas I., Durmuş A.: *Efficiency and exergy analysis of a new solar air heater*. Renew. Energ. **29**(2004), 9, 1489–501.

[26] Öztürk H.H.: *Experimental determination of energy and exergy efficiency of the solar parabolic-cooker*. Solar Energy **77**(2004), 1, 67–71.

[27] Gupta M.K., Kaushik S.C.: *Exergetic performance evaluation and parametric studies of solar air heater*. Energy **33**(2008), 1691–1702.

[28] Gupta M.K., Kaushik S.C.: *Performance evaluation of solar air heater for various artificial roughness geometries based on energy, effective and exergy efficiencies*. Renew. Energy **34**(2009), 465–476.

[29] Gupta M.K., Kaushik S.C.: *Performance evaluation of solar air heater having expanded metal mesh as artificial roughness on absorber plate*. Int. J. Therm. Sci. **48**(2009), 1007–1016.

[30] Akpinar E.K., Koçyiğit F.: *Energy and exergy analysis of a new flat-plate solar air heater having different obstacles on absorber plates*. Appl. Energy **87**(2010), 11, 3438–3450.

[31] Alta D., Bilgili E., Ertekin C,. Yaldiz O.: *Experimental investigation of three different solar air heaters: Energy and exergy analyses*. Appl. Energy **87**(2010), 10, 2953–2973.

[32] Pandey A.K., Tyagi V.V., Park S.R., Tyagi S.K.: *Comparative experimental study of solar cookers using exergy analysis*. J. Therm. Anal. Calorim. **109**(2012), 1, 425–431.

[33] Benli H.: *Experimentally derived efficiency and exergy analysis of a new solar air heater having different surface shapes*. Renew. Energy **50**(2013), 58–67.

[34] Lanjewar A, Bhagoria J.L., Sarviya R.M.: *Heat transfer and friction in solar air heater duct with W-shaped rib roughness on absorber plate*. Energy **36**(2011), 7, 4531–4541.

[35] Duffie J.A., Beckman W.A.: *Solar Engineering Thermal Processes*. Wiley, New York 1992.

[36] Altfeld K., Leiner W., Fiebig M.: *Second law optimization of flat-plate solar air heaters. Part I: The concept of net exergy flow and the modeling of solar air heaters*. Sol. Energy **41**(1988), 2, 127–132.

[37] Svirezhev Y.M., Steinborn W.H., Pomaz V.L.: *Exergy of solar radiation: global scale*. Ecol. Model. **169**(2003), 2-3, 339–346.

[38] Patela R.: *Exergy of Heat Radiation*. J. Heat Transfer **86**(1964), 2, 187–192.

[39] Singh S., Chander S., Saini J.S.: *Exergy based analysis of solar air heater having discrete V-down rib roughness on absorber plate*. Energy **37**(2012), 1, 749–758.

[40] Sahu M.K., Prasad R.K.: *Exergy based performance evaluation of solar air heater with arc-shaped wire roughened absorber plate*. Renew. Energy **96**(2016), 233–243.

[41] Klein S.A.: *Calculation of flat-plate collector loss coefficients*. Sol. Energy **17**1975), 1, 79–80.

[42] McAdams W.H.: *Heat Transmission*. McGraw-Hill, New York 1954.

[43] Karwa R., Chitoshiya G.: *Performance study of solar air heater having v-down discrete ribs on absorber plate*. Energy **55**(2013), 939–955.

[44] Swinbank W.C.: *Long-wave radiation from clear skies*. Q. J. Roy. Meteor. Soc. **89**(1963), 339–348.

[45] Gupta D., Solanki S.C., Saini J.S.: *Thermo-hydraulic performance of solar air heaters with roughened absorber plates*. Sol. Energy **61** (1997); 1, 33–42.